Satellite Microwave Surface Observations in Tropical Cyclones

YVES QUILFEN, BERTRAND CHAPRON, AND JEAN TOURNADRE

Laboratoire d'Océanographie Spatiale, IFREMER, Plouzané, France

(Manuscript received 23 April 2009, in final form 10 July 2009)

ABSTRACT

Sea surface estimates of local winds, waves, and rain-rate conditions are crucial to complement infrared/visible satellite images in estimating the strength of tropical cyclones (TCs). Satellite measurements at microwave frequencies are thus key elements of present and future observing systems. Available for more than 20 years, passive microwave measurements are very valuable but still suffer from insufficient resolution and poor wind vector retrievals in the rainy conditions encountered in and around tropical cyclones. Scatterometer and synthetic aperture radar active microwave measurements performed at the C and Ku band on board the European Remote Sensing (ERS), the Meteorological Operational (MetOp), the Quick Scatterometer (QuikSCAT), the *Environmental Satellite (Envisat)*, and RadarSat satellites can also be used to map the surface wind field in storms. Their accuracy is limited in the case of heavy rain and possible saturation of the microwave signals is reported. Altimeter dual-frequency measurements have also been shown to provide along-track information related to surface wind speed, wave height, and vertically integrated rain rate at about 6-km resolution. Although limited for operational use by their dimensional sampling, the dual-frequency capability makes altimeters a unique satellite-borne sensor to perform measurements of key surface parameters in a consistent way. To illustrate this capability two *Jason-1* altimeter passes over Hurricanes Isabel and Wilma are examined. The area of maximum TC intensity, as described by the National Hurricane Center and by the altimeter, is compared for these two cases. Altimeter surface wind speed and rainfall-rate observations are further compared with measurements performed by other remote sensors, namely, the Tropical Rainfall Measuring Mission instruments and the airborne Stepped Frequency Microwave Radiometer.

1. Introduction

Thanks to satellite-based observations, extreme weather events such as tropical cyclones (TCs) or explosive midlatitude storms and polar lows can be frequently observed and analyzed. These measurements are critical for short-term forecasting. Yet, prediction of TC intensity and potential destructiveness remains a major challenge. The Dvorak technique makes use of infrared and visible images from polar-orbiting and geostationary satellites for TC intensity analysis (Dvorak 1975). The method has been reviewed by Velden et al. (2006) to demonstrate its general adequacy but also to emphasize its inherent limitations. Conclusions led the authors to consider that aircraft reconnaissance and satellite microwave data are crucial to aid TC intensity analysis. As demonstrated by radiometers on board the Defense Meteorological Satellite Program (DMSP) satellite series, WindSat, and the Tropical Rainfall Measuring Mission (TRMM), as well as by scatterometers on board the European Remote Sensing (ERS), the Adaptive Domain Environment for Operating Systems (ADEOS), the Quick Scatterometer (QuikSCAT), and the Meteorological Operational (MetOp) satellites or synthetic aperture radars (SAR) on board the *Environmental Satellite* (*Envisat*) and *Radarsat* satellites, synoptic observations of surface wind and atmospheric water content generally reveal storm structures with impressive detail. However, most microwave sensors suffer severe limitations when attempting to retrieve the surface wind speed under extreme conditions. These limitations are linked to the ground resolution, to saturation of the signals, or to the infeasibility to separate the wind and rain signals from single-frequency measurements (Quilfen et al. 1998). Altimeter measurements are limited to nadir observations, and are seldom used for TC studies. However, up to five altimeters have recently been in operation to provide high-resolution (6 km) information when crossing a TC. While certainly limited by

Corresponding author address: Yves Quilfen, Laboratoire d'Océanographie Spatiale, IFREMER, Plouzané 29280, France.
E-mail: yves.quilfen@ifremer.fr

DOI: 10.1175/2009MWR3040.1

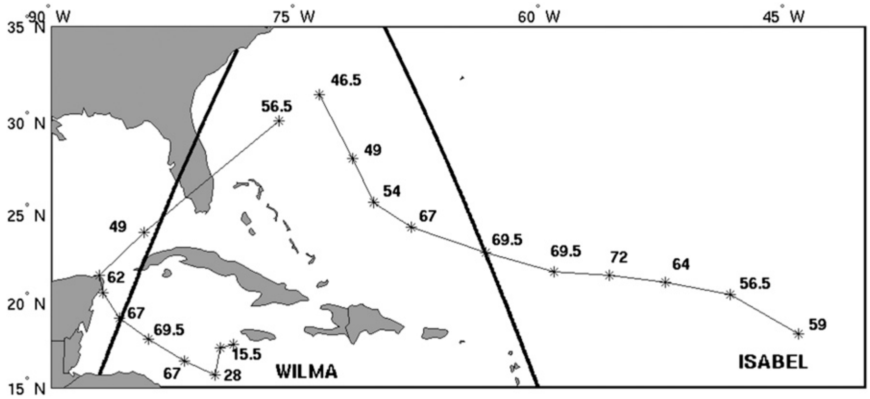

FIG. 1. The TC Isabel and Wilma best tracks (regular lines) as determined by the HRD (NOAA/AOML) and the two corresponding *Jason-1* passes (thick lines). MSWS values (stars, m s^{-1}) are values estimated each day at 0000 UTC, starting on the east side at 9 Sep 2003 for Isabel and 16 Oct 2005 for Wilma.

their relatively coarse across-track sampling, the altimeter measurements have been demonstrated to provide very valuable information (Young 1993; Quilfen et al. 2006). Moreover, thanks to their dual-frequency capability, the Ocean Topography Experiment (TOPEX)/Poseidon, *Envisat*, and *Jason-1* and *-2* altimeters signals can be processed using specialized algorithms to retrieve the surface wind speed and significant wave height, along with the rain rate in extreme weather events. In this paper, we further elaborate on these results to explore in depth these altimeter capabilities to observe and quantitatively characterize extreme events. The possibility to retrieve combined information is quite unique and the altimeter sea-state measurements provide an integrated energy estimation related to the intensity of the surface winds near the intense generation areas.

In section 2 we describe the category-5 TCs Isabel and Wilma and briefly present how the maximum sustained wind speed is estimated at the National Hurricane Center. The Isabel and Wilma examples have been chosen because they presented very different cloud patterns for the same Dvorak intensity estimate at the *Jason-1* altimeter observation times, and very different coverage by aircraft reconnaissance flights. Observability conditions were good in Isabel but poor in Wilma making the Dvorak intensity analysis somewhat difficult. In section 3, we analyze the altimeter measurements for these two TC cases. Altimeter raw waveform data and retrieved wind speed/significant wave height/rainfall-rate profiles are presented. Special attention is given to the interpretation of the observed sea state. Section 4 compares other remote sensors surface measurements with the *Jason-1* altimeter data. The results are summarized and discussed in section 5.

2. Description of TCs Isabel and Wilma

a. Isabel, Wilma, and Jason-1 *altimeter tracks*

Two altimeter tracks have been selected corresponding to the mature stages of Isabel (at 2351 UTC 13 September 2003) and Wilma (at 0154 UTC 21 October 2005). The altimeter tracks are displayed in Fig. 1 together with the best-estimate Isabel and Wilma tracks and maximum 1-min sustained wind speed (MSWS) as given in the Hurricane Database (HURDAT; Landsea et al. 2004). These values relate to the surface wind speed at 10 m above the sea surface. Because aircraft measurements are less frequent at night and unavailable in most ocean basins, satellite microwave measurements can provide invaluable information to complement the Dvorak analysis, which relies mainly on infrared measurements.

Figures 2 and 3 display the Geostationary Operational Environmental Satellite (GOES) infrared images at 6-h time step in a time window from 36 h before to 12 h after the *Jason-1* altimeter time. The GOES data are recalibrated brightness temperatures available at 8-km and 3-hourly resolution (Kossin et al. 2007). The bottom-left panels show the 6-hourly GOES infrared image closest to the time of the *Jason-1* altimeter passes. The altimeter track locations have been corrected to account for the difference between the GOES and the altimeter times (i.e., 9 min and 1 h, 54 min for Isabel and Wilma, respectively). *Jason-1* intersects the Isabel and Wilma eyes slightly on the west and southeast sides, at 7 and 15 km from the center, respectively. Figure 1 indicates that *Jason-1* crossed both cyclones in their rear-left and fore-right quadrants, the latter being where MSWS are usually encountered.

The two sets of GOES images show very different cloud and convective structure organizations. Isabel presents

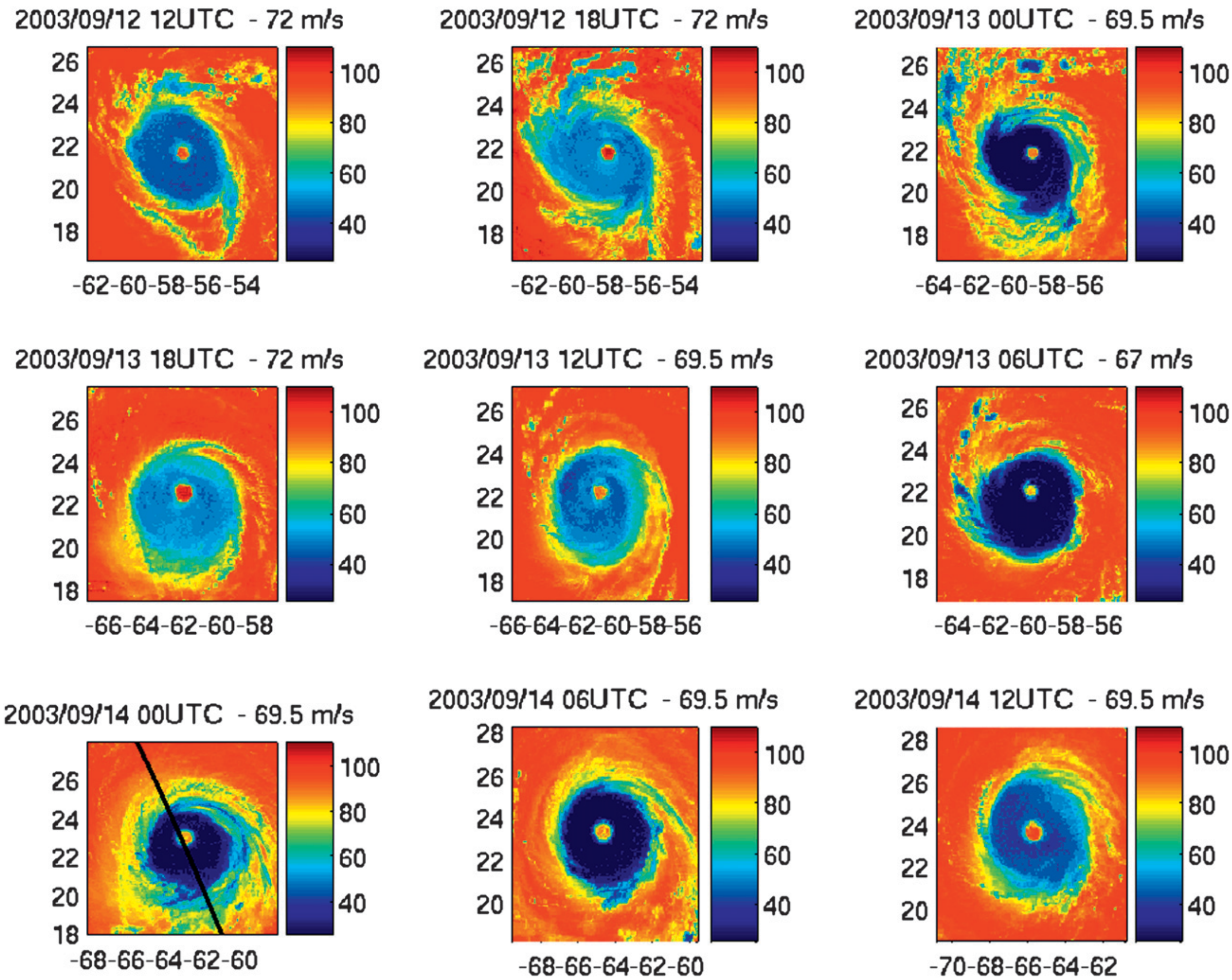

FIG. 2. Infrared brightness temperatures (K) measured by the GOES satellite every 6 h over TC Isabel from (top left) 1200 UTC 12 Sep 2003 to (bottom right) 1200 UTC 14 Sep 2003. (bottom left) The *Jason-1* track (2351 UTC 13 Sep 2003) is displayed.

a well-defined eye during the two days. It is totally or partially obscured for Wilma because its pinhole eye cannot be well resolved with the GOES images resolution. This pinhole eye is one situation where the Dvorak technique is particularly inaccurate for estimating storm intensity. The Isabel cloud patterns look symmetric while Wilma presents well-developed banding features. The cyclone intensity estimated via the Dvorak technique will then rely more on the brightness temperature difference between the warm eye and the surrounding cold cloud tops for Isabel, while it will mainly rely on analyzing the different types of observable patterns for Wilma. The Dvorak technique also relies on interpretation of the cloud patterns changes. Brightness temperatures features are very stable for Isabel the day before the *Jason-1* pass, which indicates little intensity change. Structures are evolving only slightly in Wilma with the eye becoming apparent. Uncertainties in the interpretation of such features, together with limited availability of aircraft measurements, highlight the importance of satellite microwave measurements. In particular, TRMM measurements showed the formation of a double eyewall in Wilma that corresponds to a reorganization of the convection indicating possible intensity change.

b. Maximum surface wind speed measurements and best-track analysis

Figure 4 illustrates the way the MSWS is estimated in HURDAT using GOES brightness temperatures, aircraft, and other measurements. For Isabel (Fig. 4a), MSWSs were derived mainly from the Dvorak analysis prior to 12 September. After this date, reconnaissance aircraft data were mainly used and the MSWS was set to the maximum surface wind speed among available measurements. The large dispersion at a given date is due to aircraft transects that do not necessarily cross

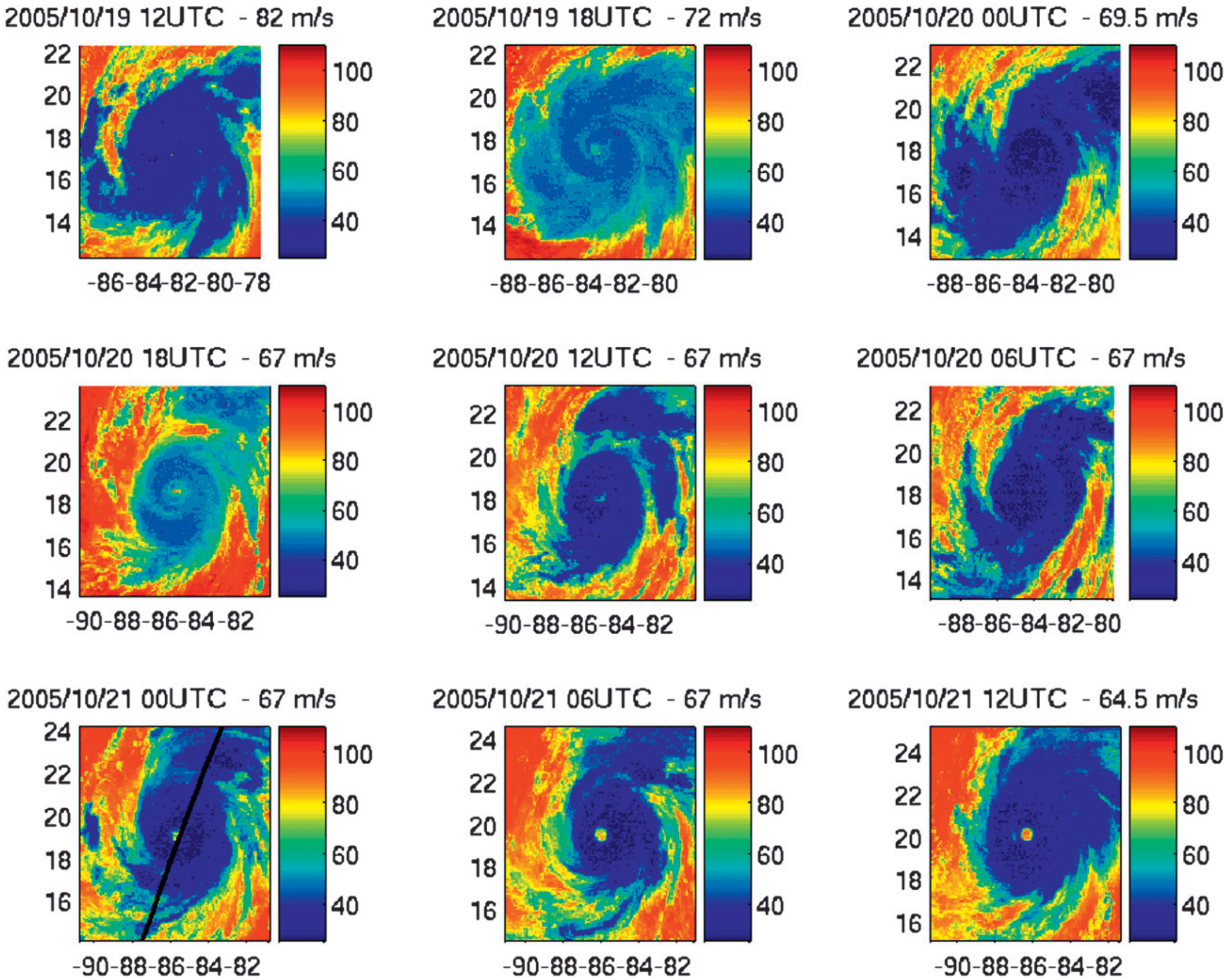

FIG. 3. Infrared brightness temperatures (K) measured by the GOES satellite every 6 h over TC Wilma from (top left) 1200 UTC 19 Oct 2005 to (bottom right) 1200 UTC 21 Oct 2005. (bottom left) The *Jason-1* track (0154 UTC 21 Oct 2005) is displayed.

the maximum wind speed area, and to the large variety of wind estimate sources. There is some disagreement between MSWSs derived from aircraft data and those derived from the Dvorak analysis, the latter being significantly lower between 13 September and 16 September. At the time of the *Jason-1* orbit, the Dvorak estimate was below 67 m s^{-1} while aircraft estimates were 72 and 69.5 m s^{-1} the day before at 1930 UTC and the day after, respectively. Flight-level winds are reduced to the surface using a constant factor. For a usual flight level of 700 hPa, the reduction factor commonly used is 10% for eyewall measurements (Franklin et al. 2003). This factor can be adjusted depending on environmental conditions, storm history, and on the observed patterns. Furthermore, a large azimuthal variability was found with larger values (close to 0.9) in the left-front quadrant and weaker values (close to 0.8) in the right-rear quadrant (Powell et al. 2009). Franklin et al. (2003) estimated the one standard deviation uncertainty on the reduction factor to be as large as 20%. When available, the dropwindsonde and Stepped Frequency Microwave Radiometer (SFMR) measurements are then given a high priority to evaluate the MSWS. SFMR data were available as part of the Coupled Boundary Layer Air–Sea Transfer (CBLAST) experiment on 12, 13, and 14 September. SFMR MSWS estimates were between 60.5 and 64.5 m s^{-1}, consistently lower than flight level and dropwindsondes estimates.

For the Wilma case (Fig. 4b), fewer aircraft data were available. Highest winds measured were 86.4 m s^{-1} at a flight level of 700 hPa on 19 October. Using a standard reduction factor of 0.9 yields a surface wind speed of 77.7 m s^{-1}. Since the central pressure was still falling, the peak intensity of Wilma is estimated to be 82.3 m s^{-1} at 1200 UTC 19 October (Pasch et al. 2006). Wilma's intensity has then decreased and best-track MSWS estimates are about 66.9 m s^{-1} for the two days before

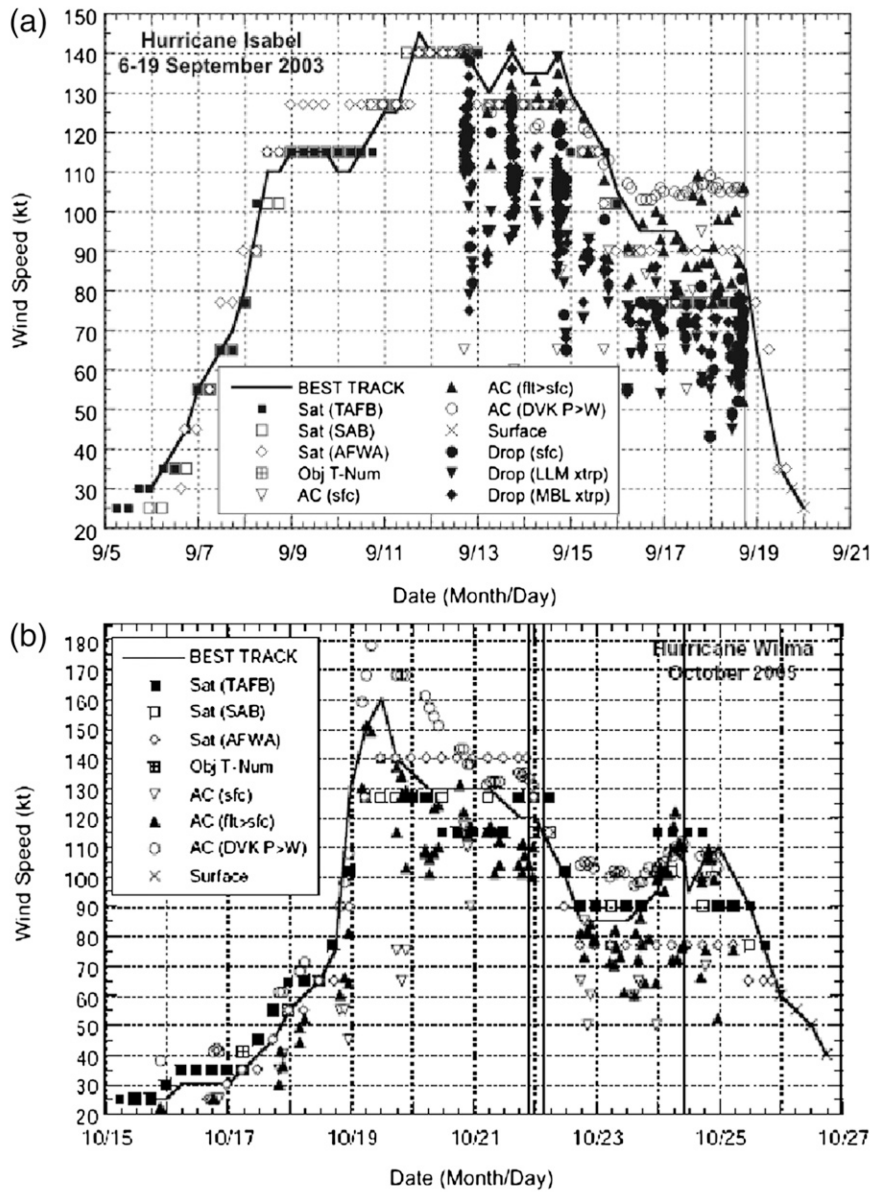

FIG. 4. Selected wind observations and best-track maximum sustained surface wind speed curve (solid line) for (top) Hurricanes Isabel (5–21 Sep 2003) and (bottom) Wilma (15–25 Oct 2005). Vertical lines denote landfalls. (From http://www.nhc.noaa.gov/.)

landfall on the Yucatan Peninsula of Mexico. There is considerable scatter between the MSWS estimates at time near the *Jason-1* pass (at 0154 UTC 21 October). Aircraft estimates were below 61.7 m s^{-1}, but Air Force Weather Agency (AFWA) Dvorak estimates remains at 72 m s^{-1}, reflecting the difficulty to evaluate the intensity changes in Wilma.

The discrepancies among the different MSWS estimates make the choice of an absolute value somewhat difficult. The root-mean-square error of the relationship between aircraft-derived and satellite-estimated minimum sea level pressures is 9 hPa (Velden et al. 2006), and further use of the Dvorak pressure–wind relationship, from which the wind is ultimately estimated, introduces far more error. The HURDAT reanalysis dealt with such issues by careful examination of all available measurements but the MSWS estimate accuracy is not characterized.

3. *Jason-1* altimeter measurements

The *Jason-1* altimeter is a nadir-looking radar operating at two frequencies, 13.6 GHz in the Ku-band and

5.3 GHz in the C-band. It performs measurements at 20-Hz sampling, the so-called waveforms representing the backscattered energy as function of time. One waveform is computed every 280 m with a footprint radius increasing roughly from 5 to 9 km with increasing wave height. Waveforms are used to compute the normalized radar cross section (σ_0) and automatic gain control (AGC) at 20- and 1-Hz sampling. AGC is a quantity linearly related to the σ_0.

The *Jason-1* satellite is a polar-orbiting satellite, such as it is convenient in the following sections to present the altimeter alongtrack profiles as a function of the latitude for qualitative comparison with GOES or TRMM images. Otherwise, the data are mapped to a storm relative coordinate system to present the results as a function of the distance from the storm center.

a. The waveform data

Figure 5 displays the waveform data for Isabel and Wilma. The speckle noise is significantly greater on the C-band data as a result of a lower transmission rate. Waveforms acquired at 20-Hz sampling rate are displayed along the *y* axis as the backscattered energy received at each telemetry bin (numbered from 1 to 104), as a function of the nadir subsatellite latitude (*x* axis). The white vertical bands indicate missing data. Data are lost when the waveform distortion is so strong that the altimeter tracker loses its lock. Missing data can thus correspond to the most extreme rainfall events. The low winds within the hurricane center, localized by the vertical black line, correspond to the waveform maxima, while the high winds and rainbands correspond to strong attenuation of the signal and thus to the waveform minima. The signals are well defined at the Ku-band, showing a small area of low winds near Wilma center and very asymmetric areas of attenuation associated to rainbands, and more symmetric features in Isabel. The differing sensitivity to rain at the Ku- and C-band is used to separate the wind and rain effects. For example in the Wilma case, it can be seen that the strong attenuation at the Ku-band near 18.2°N of latitude is not observed at the C-band.

Figure 6 displays low-order statistics on the waveform data computed at 20 and 1 Hz, as a function of latitude. The 20-Hz data do not exhibit more organized finescale variability than at 1 Hz. Although the 20-Hz signal performs a better sampling of the finer-scale features and may thus provide a better estimate of their intensity, this is not readily usable as a result of the large measurement footprint (up to 9 km) in presence of high sea states whether the measurements are made at 1 or at 20 Hz. As shown, the C-band measurements in Wilma show less attenuation patterns than the Ku-band ones, and the minimum values are not reached at the same location for Ku- and C-band measurements. This is explained by the much greater sensitivity of the Ku-band measurements to rain rate. The Ku-band minimum is thus more in line with the maximum rain rate while the C-band one is more in line with the maximum surface wind.

One important result is that Ku-band measurements exhibit little noise, to provide a continued good sensitivity to surface wind/rain rate in the most extreme conditions.

b. Wind speed, rain-rate, and wave-height retrievals

To estimate the surface wind speed, the effective (rain free) Ku- and C-band σ_0 are computed as described in Quilfen et al. (2006). It can be summarized as follows. A first estimate of Ku-band σ_0 attenuation is computed from the difference between the actual Ku-band measurement and its expected value computed using the C-band measurement and a mean empirical Ku–C-band rain-free relationship. The rainfall-rate estimate is deduced from this Ku-band attenuation using the Marshall–Palmer relationship (e.g., attenuation as a function of rain rate at different frequencies; Marshall and Palmer 1948). A C-band attenuation can then be computed to obtain a corrected C-band σ_0. A new Ku-band attenuation is then estimated and the process is iterated until the corrected Ku- and C-band σ_0 reach stable values within 0.1 dB. In this process, potential errors on estimated rainfall rates impact directly only the estimated effective C-band σ_0. The effective, rain-free, Ku-band σ_0 are then derived from the mean Ku–C-band relationship. The strength of this approach is twofold: 1) the C-band measurements are far less affected by rain than at the Ku-band, to provide reliable estimation of the attenuations (for a maximum attenuation of 10 dB at the Ku-band, the attenuation at the C-band is only 1 dB); and 2) the error on the mean Ku–C-band empirical relationship is low, decreasing with increasing wind speed to reach one standard deviation uncertainty lower than 0.2 dB. To evaluate the error structure of this process, a Monte Carlo simulation of the errors has been conducted. The bias and root-mean-square difference between the true wind and the altimeter-derived wind speed have been first computed by considering a random noise with 0.5-dB standard deviation on both the Ku- and C-band σ_0 to estimate the process accuracy, second by considering 10%, 20%, and 30% low bias on the estimated rainfall rates used to correct for the signal attenuation. The 0.5-dB value is significantly larger than the σ_0 noise value expected at less than 0.2 dB to account for unknown behavior in such extreme conditions. A maximum low bias of 30% has been selected because it is the maximum value found when comparing the altimeter and TRMM PR rainfall rates as discussed in the following section. The first simulation gives underestimation (overestimation) of the

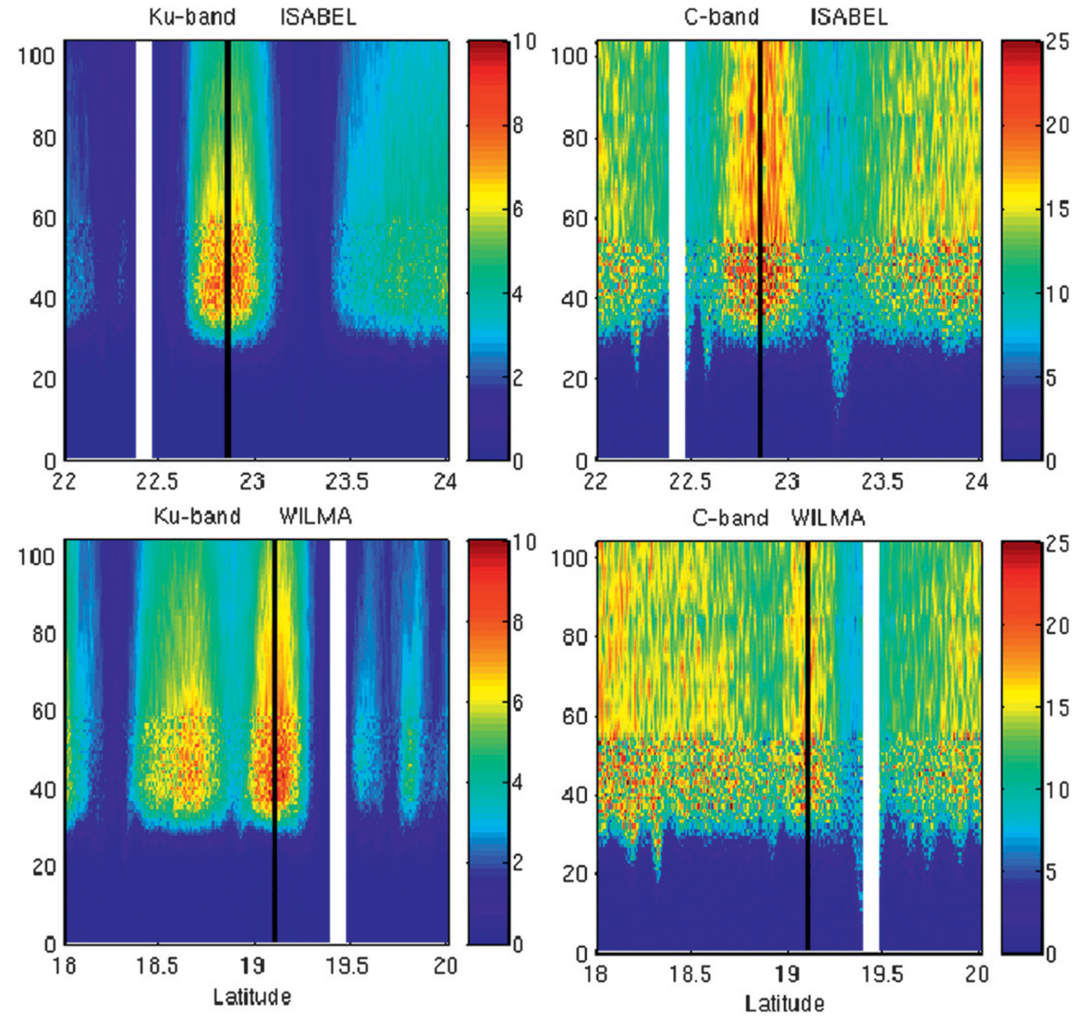

FIG. 5. Waveform as a function of the altimeter along-track latitude at 20-Hz sampling (x axis) and telemetry sample (y axis, 1 every 3.125 ms), at (left) Ku band and (right) C band for (top) Isabel and (bottom) Wilma. A waveform represents the backscattered energy as function of time (along the y axis). The echo waveform power is in an arbitrary unit. The white bars indicate missing data and the black bars indicate the location of the cyclone center.

σ_0 (wind speed) by 0.03 and 0.06 dB (0.2 and 0.4 m s^{-1}) for 10 and 20 mm h^{-1} rainfall rate, respectively. The root-mean-square difference remains lower than 0.2 m s^{-1}. The second simulation shows that underestimation of the rain rate by 10%, 20%, and 30% gives overestimation of the wind speed by 0.52, 0.78 and 1.05 m s^{-1} at 10 mm h^{-1}, by 1.34, 2.02, and 2.70 m s^{-1} at 20 mm h^{-1}, and by 2.37, 3.65 and 4.85 m s^{-1} at 30 mm h^{-1}. The results depend weakly on the wind speed. These Monte Carlo simulations mainly indicates that the wind speed retrievals are slightly impacted by a few meters per second when altimeter rain-rate estimates are biased low, but reaching about 5 m s^{-1} for the worst simulated case.

Figure 7 presents Ku- and C-band attenuation and effective σ_0 as a function of latitude. As already discussed, the areas of minimum σ_0 (maximum winds) and maximum attenuation (maximum rain rate) are not located at the same place. This indicates the tilt of the rain-rate distribution over the vertical due to the conical shape of the eyewall. This is a good indicator of the altimeter wind/rain retrieval algorithm effectiveness.

Figures 8 and 9 present the retrieved 10-min surface wind, rain rate, and significant wave height H_s, as a function of latitude for Isabel and Wilma, respectively. Using appropriate gust factors, the maximum 1-min wind is about 12% higher than the 10-min mean wind (Powell et al. 1996). The maximum 10-min surface wind speed is 49 (56) m s^{-1} for Isabel (Wilma). The 1-min equivalent altimeter wind is then 54.9 (62.7) m s^{-1} for Isabel (Wilma). The rain-rate maxima are close to 20 mm h^{-1} and the significant wave height maxima are close to 15 m, for both Isabel and Wilma.

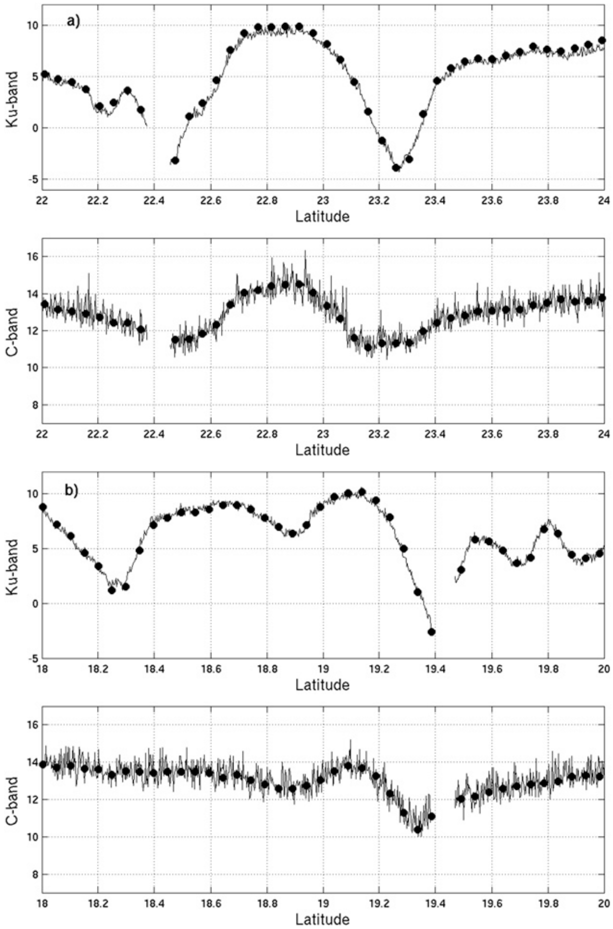

FIG. 6. Waveform maximum (solid line) and automatic gain control (dots) as a function of latitude in (a) Isabel and (b) Wilma: (top) Ku-band and (bottom) C-band data.

If an altimeter has little chance to give a reliable estimate of the MSWS giving that it may seldom overfly the peak wind (note that aircraft measurements also suffer such limitation), it can clearly provide valuable information on the surface structures. As expected, the altimeter MSWS is found in the front-right quadrant relatively to the direction of the cyclone motion for both hurricanes. Isabel presents rather symmetrical structures, as expected for a mature category 4–5 hurricane, while Wilma presents strong asymmetries in the surface wind and rainfall-rate fields. The rainfall-rate data provide critical information on convective organization whose changes are often associated with changes in the hurricane intensity (Velden et al. 2006). The TC asymmetries are determined by different factors, among which the TC intensity, its translation speed, the environmental vertical wind shear, or the gradient of planetary vorticity are preeminent (Chen et al. 2006). The stronger the TC is, the more symmetric are the rainfall structures relatively to the motion (Lonfat et al. 2004). This is verified for Isabel for which the observed asymmetries can be related to its translation speed but not for Wilma, both being at category 4 intensity at times of the *Jason-1* altimeter passes. Isabel was moving relatively fast at 12 mph while Wilma's speed was only 5 mph. This low speed can be indicative of a greater sensitivity to the vertical shear or to greater interaction with the mean flow.

One strength of the altimeters is that they perform robust companion measurements of the sea state. This provides an integrated quantity well suited to characterize the storm intensity. A review of the sea state generated by hurricanes can be found in Young (2003). Using a combined dataset from in situ buoys, synthetic aperture radars, the *Geosat* altimeter, and numerical wave prediction models, a consistent picture of a generic hurricane wave field has been obtained. Using the concept of "extended fetch," fetch-limited growth relations for the prediction of H_s are related to the maximum surface wind speed, the TC motion speed and the radius of maximum wind. This extended fetch is much larger in the area of maximum wind located in the fore right quadrant of a TC. Indeed, the waves travel in nearly the same direction as the TC in this area, and the waves are continuously fed from the wind input and can develop beyond their initial generation area. As a consequence, they grow more rapidly toward a fully developed state. At the opposite in the left quadrant of a TC where the wind waves travel mainly in the opposite direction as the TC, both wave generation and attenuation occur and the sea is more confused with a shorter fetch. It results in much smaller H_s values and much of the wave energy being from waves coming across the wind (Cline 1920; Wright et al. 2001). As shown in Fig. 1, the *Jason-1* altimeter ground track intersects these two distinctive areas of wave generation when observing Isabel and Wilma. As expected, the H_s profiles presented in Figs. 8 and 9 are more asymmetric than the corresponding wind field. This is particularly visible in Isabel. To further illustrate the consistency of the Isabel and Wilma H_s profiles with this schematic model, we also observe that the minimum H_s values are not found in the eye of the TC where the winds are the lowest.

Although defined for a MSWS range of 20–60 m s^{-1}, this model predicts a smooth saturation of the maximum possible significant wave height $H_s^{\max}$ with increasing wind speed beyond 60 m s^{-1}.

The following equation (Young 2003) predicts the maximum H_s value as follows:

$$\frac{gH_s^{\max}}{V_{\max}^2} = 0.0016\left(\frac{gx}{V_{\max}^2}\right)^{0.5},$$

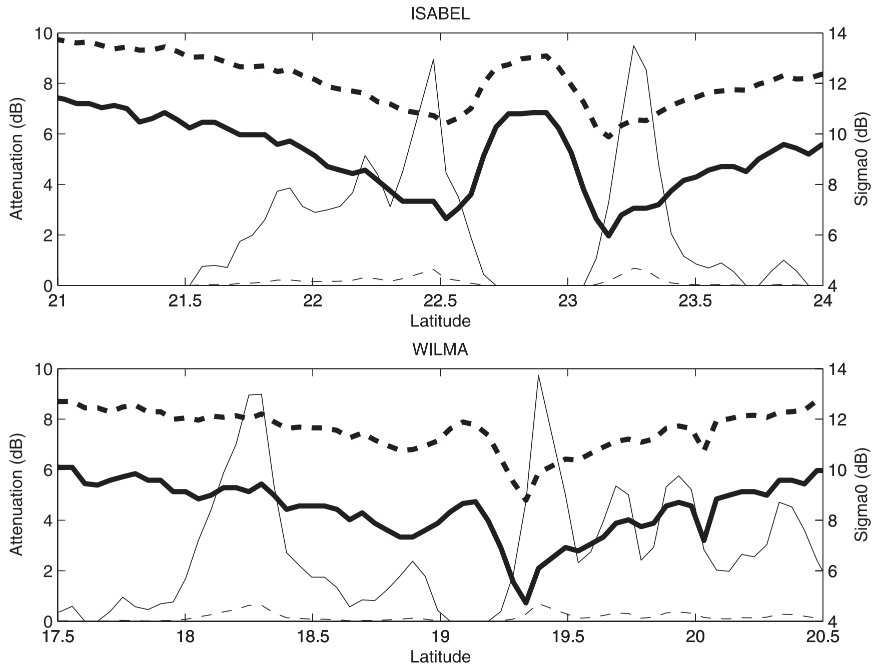

FIG. 7. Ku-band (solid lines) and C-band (dashed lines) attenuation (thin lines) and effective σ_0 (thick lines) as a function of latitude for (top) Isabel and (bottom) Wilma.

where x is called the extended fetch. Here x is defined as a nonlinear relationship, increasing with the square of the maximum wind speed $V_{\max}$, with the square of the TC motion speed, and with the logarithm of the radius of maximum wind (Young 2003). These parameters can be found in the TC extended best-track dataset (Demuth et al. 2006). Maximum wind speed (m s^{-1}), radius of maximum wind (km), and TC motion speed (m s^{-1})

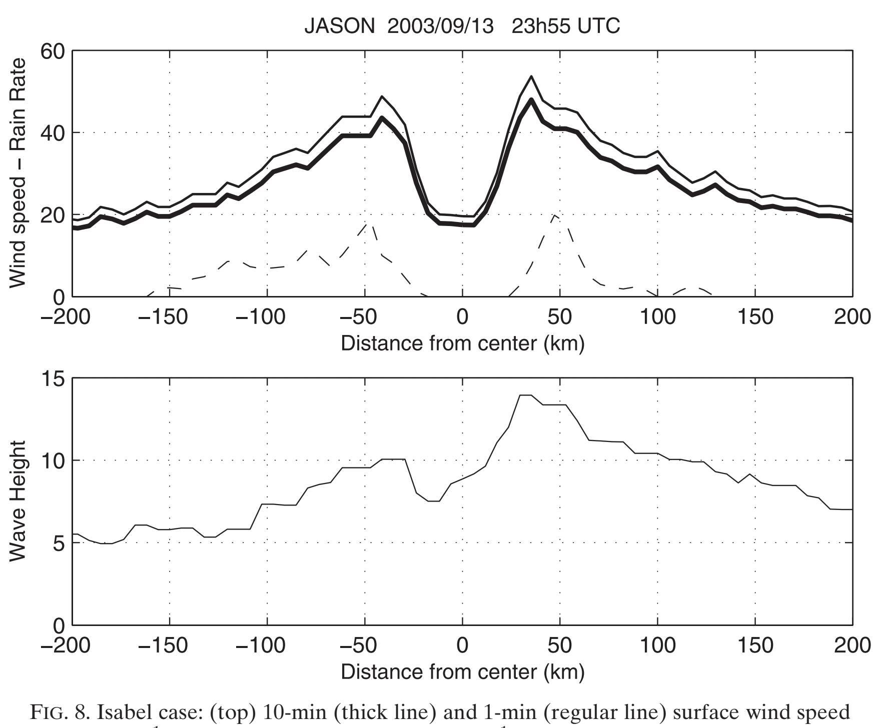

FIG. 8. Isabel case: (top) 10-min (thick line) and 1-min (regular line) surface wind speed (m s^{-1}), and rain rate (dashed line, mm h^{-1}). (bottom) Wave height (m).

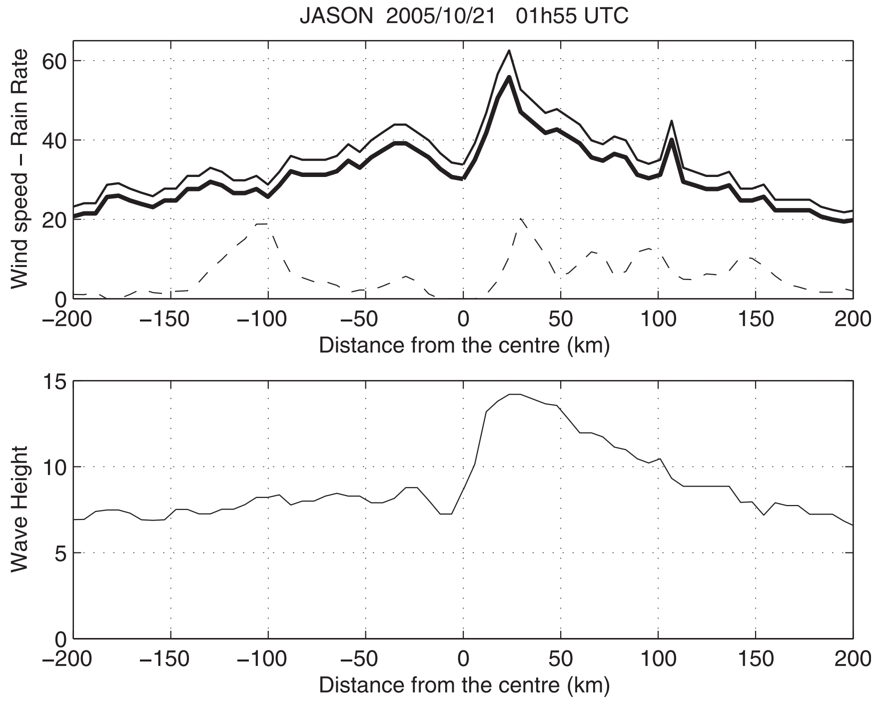

FIG. 9. As in Fig. 8, but for the Wilma case.

values are 69, 46.3, and 5.5 and 67, 37, and 2.5 for Isabel and Wilma respectively. Applications give x and $H_s^{\max}$ values of 193 km and 15.3 m for Isabel, and 118 km and 11.6 m for Wilma. The predicted $H_s^{\max}$ for Isabel is in good agreement with the altimeter measurement (14.7 m). On contrary for Wilma, it is significantly lower than the altimeter measurement (14.2 m). The model predictions reflect the underlying theory that states in particular that $H_s^{\max}$ is smaller for a slower hurricane at nearly equivalent intensity. According to the above equation, a significantly larger equivalent fetch x or $V_{\max}$ would be needed to produce the $H_s^{\max}$ measured by the altimeter in the Wilma eyewall area. Moreover, the higher sea states may have not been measured because data are missing near the right quadrant of Wilma eyewall (Fig. 5). Large errors on the estimate of x are not expected from the TC translation speed estimate since it can be determined quite accurately from satellite fixes. Estimation of the radius of maximum winds is more delicate and relies on the estimation of the eye size. However, the radius value has a rather small effect on the equivalent fetch and $H_s^{\max}$ calculation (12.2 m for $H_s^{\max}$ when using a 50-km radius for Wilma). Underestimation of the predicted $H_s^{\max}$ in the Wilma case may thus indicate that the radius of maximum wind is a poor proxy to relate with the storm size and equivalent fetch, or that MSWS significantly larger than 67 m s^{-1} would be needed to produce that high sea state. In the later case, the observed sea state may then indicate underestimation of the Wilma intensity provided in the TC extended best-track dataset. This issue certainly remains open to further investigation.

Noteworthy, *Jason-1* altimeter H_s measurements are in excellent agreement, with respect to the theoretical background developed in Young (2003), when considering the altimeter companion wind estimates along the altimeter track. Indeed, for similar $H_s^{\max}$, the altimeter $V_{\max}$ is higher for the Wilma case than for the Isabel case. Sea-state measurements could thus help to better analyze the strength of extreme events, providing an integrated quantity well suited to characterize the storm action and its strength over an area of a few tens of kilometers squared.

4. Comparison with other microwave observations

The altimeter-retrieved surface wind speed and rainfall rate can be compared to other available microwave observations to discuss the sensing capabilities and limitations of the different sensors.

a. Rain rate

The launch of TRMM has been a milestone for tropical cyclone remote sensing since it is the only sensor giving information on the rain rate vertical profile thanks

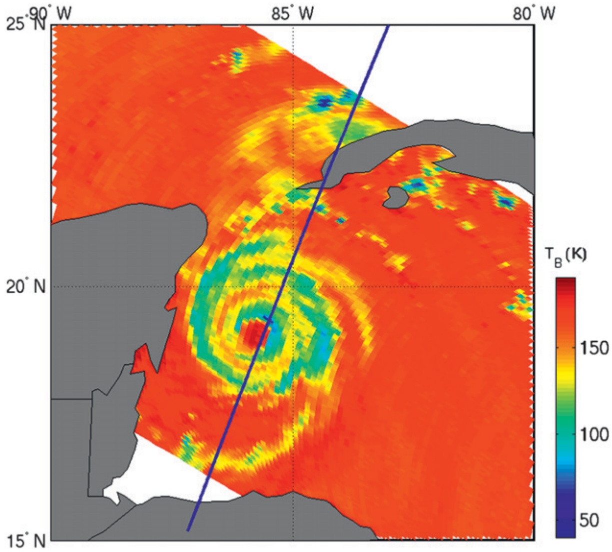

FIG. 10. The 85-GHz H-Pol TMI measurements (K) at 0055 UTC 21 Oct 2005 over TC Wilma. The blue line indicates the *Jason-1* altimeter track 1 h later.

to the precipitation radar (PR). TRMM also carries the TRMM Microwave Imager (TMI), a sensor of Special Sensor Microwave Imager (SSM/I) type, with an additional channel at 10 GHz. Figure 10 displays the 85-GHz TMI measurements at horizontal polarization at 0055 UTC 21 October, together with the *Jason-1* pass in Wilma 1 h later. The altimeter track has been shifted to account for this time difference, to show that *Jason-1* intersected Wilma slightly in the eye backside. The TMI image distinctively shows the eyewall replacement cycle, showing the erosion of the inner eyewall in its southwest side, indicating possible intensity change of Wilma.

Figure 11 displays the TRMM measurements collocated in space along the *Jason-1* pass. It accounts for the 1 h time difference by using the GOES satellite fixes at 0000 and 0003 UTC. The top panel shows the TMI 85-GHz brightness temperature T_b at horizontal polarization and the altimeter Ku-band attenuation. The TMI horizontal resolution is about 5 × 7 km at 85 GHz, similar to the *Jason-1* altimeter resolution. Altimeter attenuation estimates and TMI T_bs are well correlated, although there is some shift in the structures to be related to possible errors in space–time collocation or to the changes in the convective patterns between the TRMM and *Jason-1* times. The rapid changes in the convective activity as featured in aircraft radar images make such direct comparisons difficult. For high-frequency radiowaves, scattering by ice is significant, so that the TMI ocean rain retrieval algorithm makes use of lower frequencies to produce rainfall-rate estimates. Although the TMI rainfall-rate data are provided on the same grid as the 85-GHz channel, the use of lower channels results in smoothing and smearing of the rain structures as evidenced in Fig. 11, bottom panel. The average rainfall rate (from rain top to rain bottom) derived from the PR rainfall vertical profiles has been also displayed in Fig. 11 bottom panel, on its reduced swath compared to TMI. The 5-km resolution data have been degraded to the altimeter resolution to help comparison. We obtain a good agreement between the altimeter and the PR rainfall rates, both displaying the maximum rainfall rate in the eyewall surrounded by three other smaller maxima corresponding to the outer eyewall and rainbands.

Concerning the rainfall-rate magnitudes, one observe large discrepancies between the different rainfall estimates. The TMI and altimeter estimates are close to 20 mm h^{-1} but the maximum rainfall rate estimated by PR is close to 30 mm h^{-1}. Differences between TMI and PR rain rates have been extensively studied (Kummerow et al. 2000; Ikai and Nakamura 2003). In heavy rain cases, attenuation correction is essential to estimate the effective radar reflectivity from PR measurements. A surface reference method is used to estimate the total attenuation. It assumes that, under rain, the true radar cross section (and thus the wind and waves conditions) is the same as those in the surrounding rain-free areas (Seto and Iguchi 2007). This is clearly not the case in the eyewall region where large variations are commonly observed (e.g., in SAR images). Estimated attenuations of the PR signal in the inner eyewall (where maximum rain rate occurs) at values greater than 30 dB are thus likely to be biased as well as the derived surface rainfall rates. For the altimeter, the disagreement with the PR maximum rainfall rate has several other causes. First, the waveform tracking algorithm is not designed for such extreme conditions, resulting in a loss of data for the highest rain rates as reported in Fig. 5. Second, the altimeter attenuation to rain-rate algorithm certainly suffers limitations linked to its use for such extreme conditions (i.e., assumption of a constant rain column height and reduced sensitivity to rainfall rates greater than 20 mm h^{-1}). The quasi-linear Marshall–Palmer relationship used to retrieve the rainfall rate from the Ku-band attenuation has been calibrated for rainfall rates much lower than those encountered in tropical cyclones. Given the well-defined behavior of Ku-band radar cross section as shown in Fig. 6, a tuning of the Marshall–Palmer relation is foreseen to improve the altimeter retrievals. Note that effect of rainfall-rate underestimation on the wind speed retrieval, as described in section 3b, does not impact as much estimation of the peak wind, because the rainfall-rate and wind speed peaks are generally not coincident.

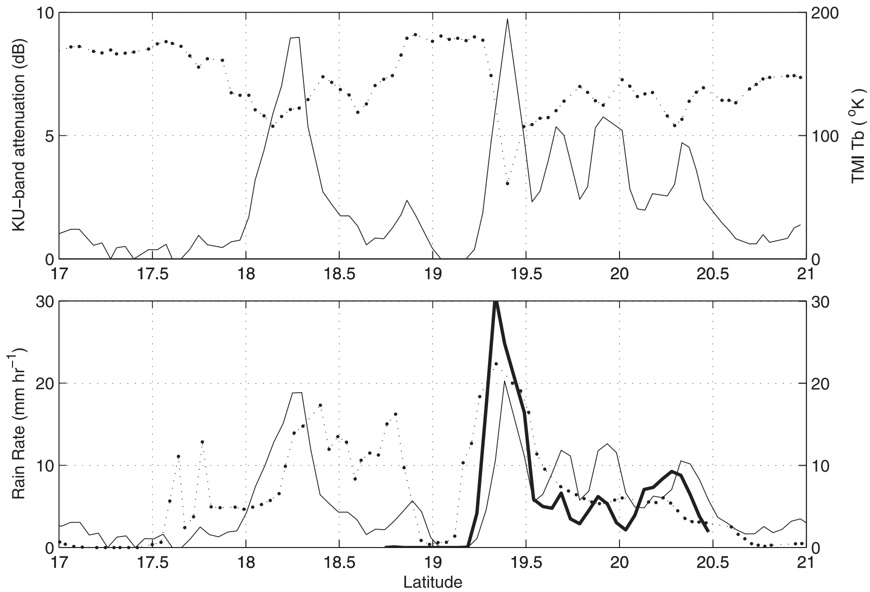

FIG. 11. (top) TMI 85-Hz H-Pol brightness temperatures (dash–dotted line) collocated with altimeter Ku-band attenuation (solid line) in TC Wilma. (bottom) TMI (dash–dotted line), *Jason-1* (solid line), and PR (thick line) rainfall rate (mm h^{-1}) in TC Wilma.

b. Wind speed

The physics of remote sensing measurements at the sea surface is still poorly understood under extreme conditions. Remote sensing at high wind speed is mostly controlled by the observation ability to directly or indirectly probe the wave breaking impacts, making passive measurements from sensors onboard SSM/I or Windsat satellites theoretically more suited for such observations (Yueh et al. 2006; Quilfen et al. 2007). However, evaluations of the ocean wind algorithms from WindSat under hurricane conditions (Adams et al. 2006) concluded that the estimated wind speed was strongly affected by atmospheric water (heavy clouds and precipitation). Furthermore, the resolution of low frequency channels for passive measurements is several tens of kilometers, which is too coarse. Active sensors have the potential to overcome this resolution issue but the surface wind field retrieval also presents unresolved issues linked to the strong signature of heavy rain and to the saturation of the scatterometer Ku- and C-band signals. Improved resolution is certainly crucial and relatively high-resolution scatterometry (~12.5 km) from *ERS-1* C-band, V-Pol, measurements has been used with success to map the evolution of the surface wind field in tropical cyclones (Quilfen et al. 1998). Thanks to its wide swath, the QuikSCAT Ku-band scatterometer has the capability to observe each tropical cyclone 1 or 2 times per day. However, rain strongly affects the Ku-band signal and contributes to its saturation at high wind speed (Tournadre and Quilfen 2003). Indeed, Ku-band rain-free measurements are shown to saturate at hurricane-force winds, faster at V-Pol than at H-Pol (Fernandez et al. 2006). If some information can be gained from very high resolution QuikSCAT measurements to better map the rain structures and to improve quantitative estimation of the rain rate/wind field (Allen and Long 2005), the authors concluded that this is not applicable in high wind/rain events. Such limitations are invoked to envisage a QuikSCAT follow-on mission carrying a dual-frequency scatterometer.

Dual-frequency altimeter measurements in TCs can be compared with measurements of the SFMR specifically operated on board National Oceanic and Atmospheric Administration (NOAA) aircraft for TC remote sensing. The SFMR instrument was experimental before 2005 when it became operational. It was not operated in Wilma on the days close to the *Jason-1* pass, but it was operated on the days before and after the *Jason-1* pass in Isabel. Figure 12 displays the SFMR leg operated in the frame of the CBLAST experiment on board the 43RF aircraft, on 13 September near 2000 UTC. It is about 4 h before the *Jason-1* time. The *Jason-1* ground track is indicated as a dashed line on the top panel, showing that it intersects the right-front quadrant of Isabel while the SFMR ground track intersects the right-rear quadrant. SFMR surface winds are displayed on the bottom panel together with the flight level winds and the SFMR surface rainfall rate. Maximum SFMR surface wind speed for this flight time is measured at 60.5 m s^{-1}, using the model function described in Powell et al. (2009). It is

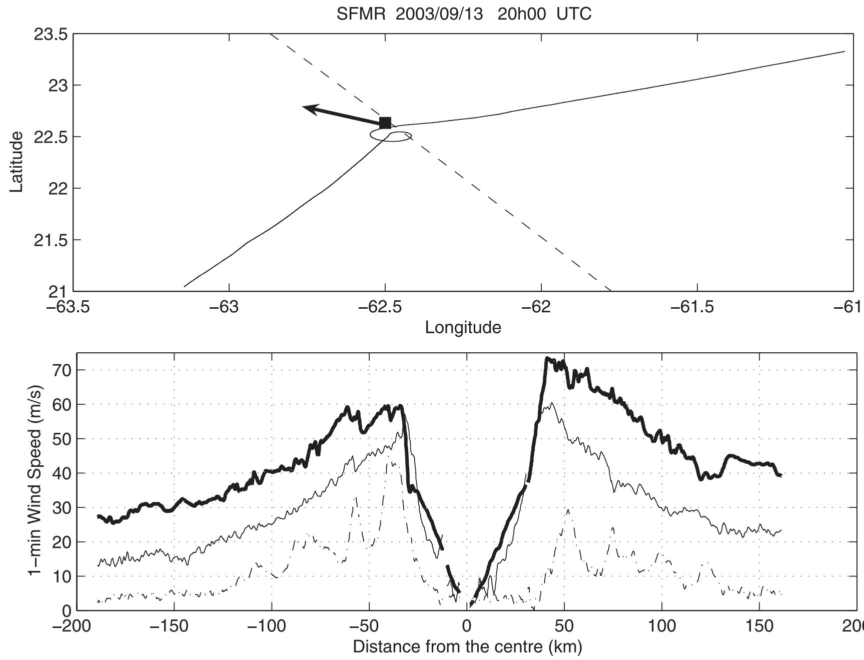

FIG. 12. (top) SFMR (solid line) and *Jason-1* (dashed line) tracks. The square and the arrow indicate the TC Isabel center and direction of motion, respectively. (bottom) SFMR surface wind speed (m s^{-1}, regular line) and rainfall rate (mm h^{-1}, dashed line), and flight level-based wind speed (m s^{-1}, thick line), as a function of the distance from the TC center.

consistently lower than the coincident aircraft flight level-based MSWS measurement at 65 m s^{-1}. A shift is observed between the MSWS and rainfall-rate maxima locations, the maximum rainfall rate being located outward and more in line with the flight level-based maximum wind than with the surface maximum wind. This is the effect of the eyewall conical shape as commonly observed (Uhlhorn and Black 2003). The same misalignment between maximum rainfall rate and maximum surface wind speed is also clearly discernible with altimeter measurements for both TCs Isabel and Wilma (Figs. 8 and 9).

The SFMR MSWS estimates from 12 to 14 September were 63 m s^{-1} at 1710 UTC 12 September; 62.7 and 60.5 m s^{-1} at 1755 and 2000 UTC 13 September, respectively; and 64.2 m s^{-1} at 1722 UTC 14 September. This variability may be associated with the effect of the passage of Isabel over TC Fabian's wake where the sea surface temperature was lower by more than 1°C. Numerical simulations show that it can correspond to a decrease in MSWS whose magnitude can oscillate between 5 and 10 m s^{-1} in the few hours following the SST drop (Bell and Montgomery 2008). Although the altimeter MSWS measured at only 55 m s^{-1} certainly indicates that the altimeter did not sample well the maximum wind area, it may also reflect these cooler SSTs since Isabel was still traveling over the Fabian's wake before encountering warmer SSTs later on 14 September.

To help interpretation of the comparison between the altimeter wind profile with the closest SFMR leg (at 2000 UTC 13 September) 4 h before the altimeter time, it is convenient to collocate both with the Hurricane Research Division (HRD) wind analysis (H*WIND). The HRD has defined this experimental wind analysis tool to provide regular high-resolution wind fields for tropical cyclones (Powell et al. 1998). Figure 13 shows the H*WIND analysis performed at the altimeter time (courtesy of M. Powell) collocated with the SFMR wind speed (top panel) and with the *Jason-1* wind speed (bottom panel). Time difference between the SFMR and the H*WIND data is accounted for by shifting spatially the SFMR measurements to match the altimeter and H*WIND time, and the SFMR data have been degraded to the H*WIND resolution (6 km). The SFMR and the altimeter agree very well with the H*WIND analysis indicating maximum wind speed as expected on the right side of Isabel. This was expected for the SFMR whose measurements are used into the H*WIND analysis. Comparison of this altimeter profile with the H*WIND analysis shows that the altimeter successfully captures the wind speed variability along its track. For operational purpose, the H*WIND analysis makes use of real-time processed SFMR data whereas the SFMR data presented Fig. 13 are postprocessed data using the latest wind algorithm (Powell et al. 2009). This is why the

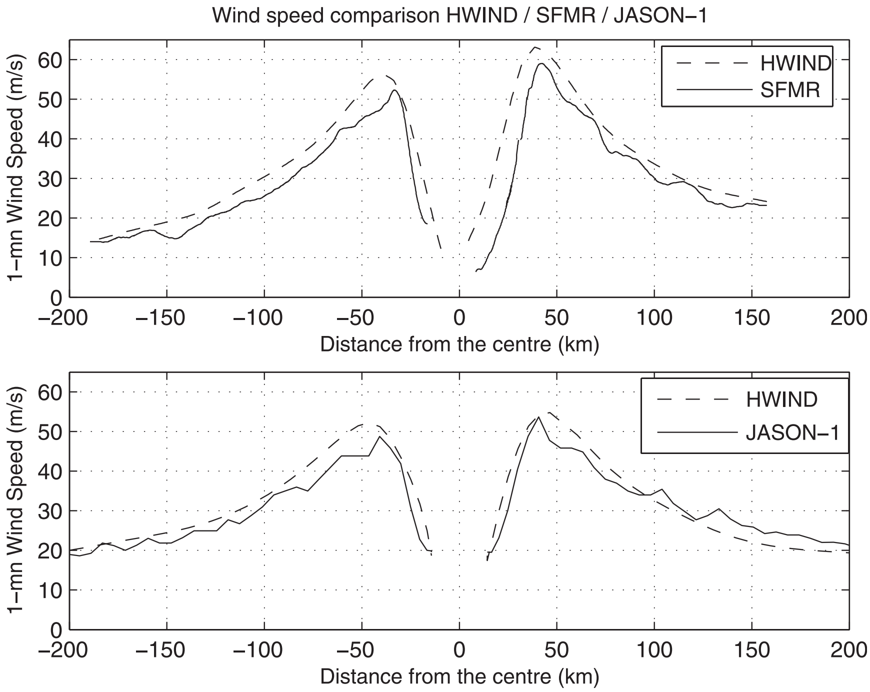

FIG. 13. (top) SFMR (solid line, 2000 UTC 13 Sep 2003) and H*WIND (dashed line, 2355 UTC 13 Sep 2003) wind speed (m s^{-1}). (bottom) *Jason-1* (solid line, 2351 UTC 13 Sep 2003) and H*WIND (dashed line, 2355 UTC 13 Sep 2003) wind speed (m s^{-1}). Positive values of the distance are associated with the right side of Isabel.

SFMR wind speed is lower than the H*WIND one. The altimeter wind profile would thus be closer to the H*WIND one if the latest SFMR algorithm had been used to produce the H*WIND field. Other reasons can be invoked for this apparent altimeter wind speed underestimation. First, the H*WIND analysis may not account properly for a possible decrease of Isabel intensity at this time as it traveled across the Fabian's wake. Indeed the H*WIND maximum wind speed is derived from the SFMR maximum wind speed valid 6 h before. Second, the altimeter wind retrieval empirical algorithm is a linear relationship between the surface wind speed and the Ku-band radar cross section showing a decrease rate of 0.156 dB each m s^{-1} (Young 1993). It has been derived using *Geosat* altimeter monofrequency measurements mapped to the Holland wind field empirical model (Holland 1980) for only six altimeter passes through a tropical cyclone. The area of maximum wind is generally associated with rainfall but the *Geosat* measurements were not edited for rain impacted measurements. As shown in Fig. 6, the *Jason-1* dual-frequency measurements indicate that Ku-band measurements are strongly attenuated near the cyclone eyewall. It means that wind speed values predicted by the Young model are likely to be systematically underestimated in the high wind speed region, leading to systematic underestimation of the wind speed. This may thus partly explain the observed *Jason-1* wind speed underprediction as shown in Fig. 13.

Apart the difference in maximum wind intensity, the surface wind profiles derived from the SFMR and from the altimeter are in very good agreement. Interestingly, the SFMR and the altimeter wind profiles present the same behavior near the rain-rate peaks on both sides of Isabel's eye. Whether it is geophysically consistent or it originates from the rain/wind retrieval algorithms has not been analyzed.

The availability of more than 15 yr of dual-frequency altimeter measurements, together with the continuous improvement of TC intensities estimates, is a motivation to revisit the altimeter wind speed retrieval algorithm to better exploit the altimeters dual-frequency capabilities.

5. Summary

a. Results

Surface measurements in TCs are difficult to obtain and only microwave sensors below 15 GHz can penetrate the deep convective clouds surrounding the areas where surface winds are the largest. These kind of measurements are crucial to complement the Dvorak TC intensity analysis as obtained from infrared/visible measurements.

Moreover, multifrequency measurements are needed to separate wind and rain effects in intense rainy areas.

We analyze in this study the ability of *Jason-1* dual-frequency altimeter measurements to provide estimates of surface winds, waves, and rainfall rate in the case of two category-5 hurricanes. Isabel and Wilma are particularly interesting to present very different structures (eye size and visibility, asymmetries), although scaled at the same intensity at the time of *Jason-1* overflight. This offers a good test bed to show that the altimeter can be used to distinguish such features. Variability of the surface wind speed and rainfall rate is well characterized along the altimeter ground track. As expected from the eyewall conical shape, the maximum rainfall rate occurs slightly more outward than the maximum surface wind speed (MSWS). Contrary to Wilma showing an eyewall replacement cycle at the altimeter observation time, Isabel MSWS and rain-rate structures are very symmetric. Altimeter measurements in Isabel are compared with the SFMR measurements and with the HRD wind analysis, showing good agreement of the wind profiles but underestimation of the SFMR and altimeter winds by comparison with the HRD ones. In the Wilma case, there are no direct surface measurements to compare with the altimeter. Altimeter MSWS estimate at 62.7 m s^{-1} may not coincide with the peak wind estimated at 67 m s^{-1} from flight level-based measurements in the best-track reanalysis. However, estimated altimeter MSWS values are suggested to be biased low because of the rather large footprint (~8 or 9 km) in high sea-state conditions and because the wind speed retrieval empirical model may underpredict the radar cross section at the high wind speed encountered in the rainy areas of the TC eyewalls. The availability of more than 15 yr of dual-frequency altimeter measurements, together with the continuous improvement of TC intensities estimates, is a motivation to revisit the original work performed by Young (1993) to better exploit the modern altimeter dual-frequency capabilities.

We also present the unique altimeter capability to perform companion sea-state measurements. The sea state accounts for space–time-integrated effects of the storm action and H_s measurements can thus partially limit effects of the poor altimeter sampling. We compare the altimeter H_s measurements with values predicted by a parametric model to interpret the observed sea state. Maximum H_s generated in the field of a TC can be predicted using this model and estimates of the speed of the storm, the MSWS, and the radius of maximum winds. The predicted $H_s^{\max}$ at 15.3 m for Isabel is in good agreement with the altimeter measurement at 14.7 m. For Wilma, it is significantly lower at 11.6 m than the altimeter measurement at 14.2 m. Accordingly, a significantly larger equivalent fetch x would be needed to produce the $H_s^{\max}$ measured by the *Jason-1* altimeter for the Wilma case. The observed sea state may thus indicate underestimation of the Wilma intensity estimate provided in the TC extended best-track dataset, or the fact that the radius of maximum wind is a poor proxy for a TC size as commonly used in the wind and wave parametric models. This remains open to further investigation. Sea-state measurements can help to better analyze the strength of extreme events, especially when usual methodologies using aircraft or geostationary satellites measurements are less applicable. It provides an integrated quantity well suited to characterize the storm action and its strength over an area of a few tens of kilometers. However, wide-swath sea-state sensors with better coverage of the active TC areas will be more adapted to provide useful operational information.

Rainfall rates deduced from the altimeter measurements are compared from those derived from the TRMM instruments. Good qualitative agreement is found with the Precipitation Radar data but the altimeter maximum rainfall rates in the TC eyewall are significantly lower. Given the well-defined behavior of Ku-band radar cross section, a tuning of the Marshall–Palmer relationship is suggested to improve the rainfall-rate altimeter retrievals.

b. Discussion

Instruments, as well as physical and empirical models used to interpret microwave measurements are generally developed to account for mechanisms taking place under average weather conditions. Under high wind conditions, the sea surface is no longer simply related to the wind speed. In winds approaching hurricane strength, an enhanced wave breaking activity is taking place at the surface of the ocean. Whitecap bubbles and sea spray provide additional surfaces and volumes that impact the transfer of any quantity normally exchanged at the air–sea interface. As can be expected under extreme wind forcing, breaking waves are distributed over a wider range of surface wave scales compared to milder conditions. In particular, the sea state is generally under developed and larger gravity waves are involved in breaking processes. Both foam coverage and foam thickness will significantly increase with increasing wind speeds (Reul and Chapron 2003). Furthermore, spume drops torn off breaking crests are sprayed inside the airflow at higher height (i.e., the larger-scale mean height) to possibly significantly affect the turbulent mixing. This latter effect can then lead to acceleration of the airflow and reduction of the surface drag, as suggested by wind profiles measurements under hurricane wind conditions. Consequently, ocean surface passive remote sensing measurements at very high wind speeds are certainly well adapted. However, emissivity models as well as measurements predict saturation in foam emissivity (i.e., foam approaches the behavior of a blackbody for sea-foam thickness larger than about twice the electromagnetic wavelength). Passive measurements below 15 GHz are thus expected to provide the most interesting measurements under very high wind speeds, as confirmed by the WindSat (Quilfen et al. 2007; Adams et al. 2006) and SFMR (Uhlhorn et al. 2007) measurements.

At low incidence angles, the large wave breaking signatures as well as foam and bubble impact on the ocean surface dielectric properties have apparently been successfully captured with the reported altimeter measurements. An exact interpretation is far to be completed. It can certainly be advanced that reflectivity is strongly impacted by foam layers and whitecap coverage. Increasing winds and underdeveloped sea-state conditions will also lead to steeper large gravity waves increasing the overall slope variances. Increased slope variances will lower the nadir backscatter signals at any radar frequency. According to the theory of electromagnetic waves propagating in stratified media, foam thickness will induce the total reflectivity to decrease with increasing wavelength (i.e., the Ku band is anticipated to be more attenuated than the C band). Furthermore, sea spray production is also likely to increase and saturate the atmospheric boundary layer under hurricane conditions. While sea spray production may alter the turbulent kinetic energy and turbulence in the atmospheric boundary layer to modify the overall stress at the surface, the droplet size and concentration may also impact the electromagnetic reflectivity. As for the rain attenuation, this new phase medium consisting of air and water is likely to attenuate the Ku-band more significantly than the C-band nadir microwave measurements. This is confirmed over the selected *Jason-1* tracks. First assumed to be associated to changes in surface roughness, the observed increased sensitivity for Ku-band measurements likely include foam and sea spray effects linked to airflow separation and wave breaking events. Interestingly, a very consistent sensitivity to wind beyond 20 m s^{-1} is obtained.

Acknowledgments. The authors thank the NOAA scientists for their help with the HURDAT and SFMR datasets, especially Mike Powell who did a special H*WIND reanalysis to improve the paper, and Doug Vandemark for his comments and suggestions.

REFERENCES

Adams, I. S., C. C. Hennon, W. L. Jones, and K. A. Ahmad, 2006: Evaluation of hurricane ocean vector winds from Windsat. *IEEE Trans. Geosci. Remote Sens.,* **44,** 656–666.

Allen, J. R., and D. Long, 2005: An analysis of SeaWinds-based rain retrieval in severe weather events. *IEEE Trans. Geosci. Remote Sens.,* **43,** 2870–2878.

Bell, M. M., and M. T. Montgomery, 2008: Observed structure, evolution, and potential intensity of category 5 Hurricane Isabel (2003) from 12 to 14 September. *Mon. Wea. Rev.,* **136,** 2023–2046.

Chen, S., J. Knaff, and F. Marks, 2006: Effects of vertical wind shear and storm motion on tropical cyclone rainfall asymmetries deduced from TRMM. *Mon. Wea. Rev.,* **134,** 3190–3208.

Cline, I. M., 1920: Relations of the changes in storm tides on the coast of the Gulf of Mexico to the center and movement of hurricanes. *Mon. Wea. Rev.,* **48,** 127–146.

Demuth, J., M. DeMaria, and J. Knaff, 2006: Improvement of Advanced Microwave Sounder Unit tropical cyclone intensity and size estimation algorithms. *J. Appl. Meteor. Climatol.,* **45,** 1573–1581.

Dvorak, V. F., 1975: Tropical cyclone intensity analysis and forecasting from satellite imagery. *Mon. Wea. Rev.,* **103,** 420–430.

Fernandez, D. E., J. R. Carswell, S. Frasier, P. S. Chang, P. G. Black, and F. D. Marks, 2006: Dual-polarized C- and Ku-band ocean backscatter response to hurricane-force winds. *J. Geophys. Res.,* **111,** C08013, doi:10.1029/2005JC003048.

Franklin, J. L., M. Black, and K. Valde, 2003: GPS dropwindsonde wind profiles in hurricanes and their operational implications. *Wea. Forecasting,* **18,** 32–44.

Holland, G., 1980: An analytical model of the wind and pressure profiles in hurricanes. *Mon. Wea. Rev.,* **108,** 1212–1218.

Ikai, J., and K. Nakamura, 2003: Comparison of rain rates over the ocean derived from TRMM Microwave Imager and Precipitation Radar. *J. Atmos. Oceanic Technol.,* **20,** 1709–1726.

Kossin, J. P., K. R. Knapp, D. J. Vimont, R. J. Murnane, and B. A. Harper, 2007: A globally consistent reanalysis of hurricane variability and trends. *Geophys. Res. Lett.,* **34,** L04815, doi:10.1029/2006GL028836.

Kummerow, C., and Coauthors, 2000: The status of the Tropical Rainfall Measuring Mission (TRMM) after two years in orbit. *J. Appl. Meteor.,* **39,** 1965–1982.

Landsea, C., and Coauthors, 2004: Hurricanes and typhoons: Past, present and future. *The Atlantic Hurricane Database Re-Analysis Project: Documentation for the 1851–1910 Alterations and Additions to the HURDAT Database,* R. J. Murname and K. B. Liu, Eds., Columbia University Press, 177–221.

Lonfat, M., F. Marks, and S. Chen, 2004: Precipitation distribution in tropical cyclones using the Tropical Rainfall Measuring Mission (TRMM) microwave imager: A global perspective. *Mon. Wea. Rev.,* **132,** 1645–1660.

Marshall, J., and W. M. Palmer, 1948: The distribution of raindrops with size. *J. Meteor.,* **5,** 165–166.

Pasch, R. J., E. S. Blake, H. D. Cobb III, and D. P. Roberts, 2006: Tropical Cyclone Report, Hurricane Wilma, 15–25 October 2005. National Hurricane Center, 27 pp. [Available online at http://www.nhc.noaa.gov/pdf/TCR-AL252005_Wilma.pdf.]

Powell, M. D., S. H. Houston, and T. A. Reinhold, 1996: Hurricane Andrew's landfall in south Florida. Part I: Standardizing measurements for documentation of surface wind fields. *Wea. Forecasting,* **11,** 304–328.

——, ——, L. R. Amat, and N. Morisseau-Leroy, 1998: The HRD real-time hurricane wind analysis system. *J. Wind Eng. Ind. Aerodyn.,* **77–78,** 53–64.

——, E. Uhlhorn, and J. Kepert, 2009: Estimating maximum surface winds from hurricane reconnaissance measurements. *Wea. Forecasting,* **24,** 868–883.

Quilfen, Y., B. Chapron, T. Elfouhaily, K. Katsaros, and J. Tournadre, 1998: Observation of tropical cyclones by high-resolution scatterometry. *J. Geophys. Res.,* **103,** 7767–7786.

——, J. Tournadre, and B. Chapron, 2006: Altimeter dual-frequency observations of surface winds, waves, and rain rate in tropical cyclone Isabel. *J. Geophys. Res.,* **111,** C01004, doi:10.1029/2005JC003068.

——, C. Prigent, B. Chapron, A. A. Mouche, and N. Houti, 2007: The potential of QuikSCAT and WindSat observations for the estimation of sea surface wind vector under severe weather conditions. *J. Geophys. Res.,* **112,** C09023, doi:10.1029/2007JC004163.

Reul, N., and B. Chapron, 2003: A model of sea-foam thickness distribution for passive microwave remote sensing applications. *J. Geophys. Res.,* **108,** 3321, doi:10.1029/2003JC001887.

Seto, S., and T. Iguchi, 2007: Rainfall-induced changes in actual surface backscattering cross sections and effects on rain-rate estimates by spaceborne precipitation radar. *J. Atmos. Oceanic Technol.,* **24,** 1693–1709.

Tournadre, J., and Y. Quilfen, 2003: Impact of rain cell on scatterometer data: 1. Theory and modeling. *J. Geophys. Res.,* **108,** 2003, doi:10.1029/2002JC001428.

Uhlhorn, E. W., and P. G. Black, 2003: Verification of remotely sensed sea surface winds in hurricanes. *J. Atmos. Oceanic Technol.,* **20,** 99–116.

——, ——, J. L. Franklin, M. Goodberlet, J. Carswell, and A. S. Goldstein, 2007: Hurricane surface wind measurements from an operational stepped frequency microwave radiometer. *Mon. Wea. Rev.,* **135,** 3070–3085.

Velden, C., and Coauthors, 2006: The Dvorak tropical cyclone intensity estimation technique: A satellite-based method that has endured for over 30 years. *Bull. Amer. Meteor. Soc.,* **87,** 1195–1210.

Wright, C. W., and Coauthors, 2001: Hurricane directional wave spectrum spatial variation in the open ocean. *J. Phys. Oceanogr.,* **31,** 2472–2488.

Young, I. R., 1993: An estimate of the Geosat altimeter wind speed algorithm at high wind speeds. *J. Geophys. Res.,* **98,** 20 275–20 285.

——, 2003: A review of the sea state generated by hurricanes. *Mar. Struct.,* **16,** 201–218.

Yueh, S. H., W. J. Wilson, S. J. Dinardo, and S. V. Hsiao, 2006: Polarimetric microwave wind radiometer model function and retrieval testing for WindSat. *IEEE Trans. Geosci. Remote Sens.,* **44,** 584–595.